HHS Public Access

Author manuscript

Lab Chip. Author manuscript; available in PMC 2015 October 21.

Published in final edited form as:

Lab Chip. 2014 October 21; 14(20): 3925–3936. doi:10.1039/c4lc00688g.

Human Airway Musculature on a Chip: An In Vitro Model of Allergic Asthmatic Bronchoconstriction and Bronchodilation

Alexander P. Nesmith, **Ashutosh Agarwal**, **Megan L. McCain**, and **Kevin Kit Parker***

Disease Biophysics Group, Wyss Institute for Biologically Inspired Engineering and the School of Engineering and Applied Sciences, Harvard University, Cambridge, MA 02138 USA

Abstract

Many potential new asthma therapies that show promise in the pre-clinical stage of drug development do not demonstrate efficacy during clinical trials. One factor contributing to this problem is the lack of human-relevant models of the airway that recapitulate the tissue-level structural and functional phenotypes of asthma. Hence, we sought to build a model of a human airway musculature on a chip that simulates healthy and asthmatic bronchoconstriction and bronchodilation *in vitro* by engineering anisotropic, laminar bronchial smooth muscle tissue on elastomeric thin films. In response to a cholinergic agonist, the muscle layer contracts and induces thin film bending, which serves as an *in vitro* analogue for bronchoconstriction. To mimic asthmatic inflammation, we exposed the engineered tissues to interleukin-13, which resulted in hypercontractility and altered relaxation in response to cholinergic challenge, similar to responses observed clinically in asthmatic patients as well as in studies with animal tissue. Moreover, we reversed asthmatic hypercontraction using a muscarinic antagonist and a β-agonist which are used clinically to relax constricted airways. Importantly, we demonstrated that targeting RhoA-mediated contraction using HA1077 decreased basal tone, prevented hypercontraction, and improved relaxation of the engineered tissues exposed to IL-13. These data suggest that we can recapitulate the structural and functional hallmarks of human asthmatic musculature on a chip, including responses to drug treatments for evaluation of safety and efficacy of new drugs. Further, our airway musculature on a chip provides an important tool for enabling mechanism-based search for new therapeutic targets through the ability to evaluate engineered muscle at the levels of protein expression, tissue structure, and tissue function.

Introduction

Asthma is a leading cause of emergency department visits and hospitalization in pediatric populations[1]. In allergic asthma, the clinical symptoms of coughing, wheezing, and breathlessness result from an exaggerated increase in smooth muscle tone in response to allergen provocation of the immune system[2, 3]. Current therapeutic strategies target inflammation using glucocorticoids and excessive airway narrowing with β agonists[4]. Unfortunately, many patients remain resistant to these treatments and are at greater risk for exacerbation[5–7]. Despite this sizable clinical problem, only two new classes of airway drugs

Corresponding Author: Kevin Kit Parker, Harvard School of Engineering and Applied Sciences, 29 Oxford St, Pierce Hall 321, Cambridge, MA 02138, Phone: 617-495-2850, Fax: 617-496-1793, kkparker@seas.harvard.edu.

have been approved by the FDA in the last thirty years: anti-leukotrienes and anti-IgE antibodies[8]. This suggests an emergent need to accelerate the pipeline for discovery and validation of airway drugs.

Preclinical studies for therapies against diseases such as asthma are traditionally performed using animal models that may present translational challenges due to interspecies differences[9, 10]. In addition to animal models, there are several *ex vivo* and *in vitro* approaches to assess the contractility of airway smooth muscle (ASM) in response to the allergic immune response observed in asthma. Airway smooth muscle strips and rings mounted on force transducers are advantageous for studying tissue-level structure and contractility, but the assays are lower-throughput and human tissue supply is scarce [11]. In addition, magnetic twisting cytometry and traction force microscopy are effective tools for studying the effects of chemical, mechanical, and pharmacological stimuli on cellular stiffness and cellular force generation, respectively[12, 13, 14]. However, it remains unclear how to extrapolate the single cell data obtained from these studies to tissue-level structural and functional responses to drugs[13, 14]. Three dimensional ASM-fibroblast microtissues have been fabricated and exhibited basal tone, active contraction, and relaxation, but have not yet been used to model disease[15]. Hence, we sought to develop a robust, functional, human-relevant model that can be used for screening new therapies against asthma.

We hypothesized that we could build a model of a human airway musculature on a chip that recapitulates healthy and asthmatic bronchoconstriction and bronchodilation *in vitro*. We recapitulated the simplest structural and functional unit of the human airway by engineering anisotropic human bronchial smooth muscle (BSM) lamellae and mimicked the local immune response in the asthmatic airway by exposing the engineered tissue to interleukin-13 (IL-13), a cytokine prominently found in the airway of asthmatic patients [16, 17]. IL-13 caused an increase in the expression of proteins in the RhoA/ROCK2 pathway, increased co-alignment of actin fibers within the tissue, and elicited hyperresponsiveness to acetylcholine, similar to results seen both in clinical studies and animal models. We reversed hypercontraction using standard therapies as well as a recently proposed strategy such as treatment with a rho kinase inhibitor. Lastly, we prevented hypercontraction using a rho kinase inhibitor prior to induction of contraction, demonstrating the utility of our *in vitro* model as a means for evaluating new pharmaceutical compounds, identifying disease mechanisms, and performing mechanism-based searches for therapeutics.

Results

Mimicking allergic asthma with a human airway on a chip

The human airway consists of anisotropic smooth muscle layers that wrap circumferentially around the lumen and contract and relax to decrease and increase its diameter, respectively (Fig. 1A). To recapitulate the architecture and contraction of BSM *in vitro*, we designed an airway musculature chip that consists of human bronchial smooth muscular thin films (bMTF). bMTFs comprise a bottom layer of the elastic polymer polydimethylsiloxane (PDMS) and a top layer of engineered BSM (Fig. 1B) [18, 19]. When the muscle layer contracts, the bMTF bends reducing the radius of curvature of the tissue. The bMTF chips

were fabricated on glass coverslips by spincoating a layer of the temperature-sensitive polymer poly(N-isopropylacrylamide) (pNIPAAM) within spatially defined regions, spincoating a layer of PDMS [19–23], and laser engraving arrays of cantilevers [23] (Fig. 1B and Fig. S1A). Using microcontact printing, a fibronectin pattern of 15 μm wide lines with 2 μm spaces was transferred to the PDMS substrate to enable cellular adhesion and anisotropic tissue formation (SM). Normal human primary BSM cells in growth medium were then seeded on to the micropatterned lines, promoting self-assembly of anisotropic monolayers that recapitulate the lamellar muscle architecture of the airway.

IL-13 is a cytokine prominently found in the airway of asthmatic patients and is known to contribute to increased constriction of the airway as well as structural remodeling[6]. To induce an allergic asthma phenotype in our engineered BSM, growth medium was replaced with serum-free medium to induce the switch to a physiological, contractile phenotype for 24 hours. Next, IL-13 was administered to the anisotropic, laminar BSM for an additional 10–14 hours (Fig. 1C). When tissue was ready for experiments, the bMTF chip was transferred to Tyrode's solution and the bMTFs were peeled from the substrate. The temperature was briefly dropped below 32°C to allow pNIPAAM to dissolve and to leave a freestanding, cantilevered film. The film assumed an initial curvature corresponding to the basal tone within the tissue (Fig. 1B–C). Active contraction of the BSM was induced by directly adding the cholinergic agonist acetylcholine, which is natively secreted from autonomic innervation of the bronchi, causing the film to curl further over a time scale of minutes (Fig. 1B–C). Tissue stresses were derived from observing the extent of bMTF bending and hence our chip provides quantitative measurements of basal tone and active contraction in engineered human tissue.

We asked if we could mimic an allergic bronchoconstriction on our chip. Clinically, airway hypersensitivity and hyperresponsiveness are assessed using spirometry, where the maximal forced expiratory volume (FEV) and the forced expiratory volume in one second (FEV1) are measured[24, 25]. In this diagnostic test, bronchoconstriction is elicited using a cholinergic agonist and changes in the FEV and FEV1 are measured as a result of the smooth muscle contraction and subsequent airway narrowing. Asthmatic patients experience a significant decrease in their FEV1 compared to healthy patients[26], suggesting excessive airway narrowing due to BSM contraction leading to coughing and wheezing. To test whether we could mimic allergic asthma bronchoconstriction *in vitro*, we simulated this diagnostic test by quantifying the contractile stresses of bMTFs in response to increasing concentrations of the bronchoconstrictor acetylcholine. Contraction of tissues was elicited by cumulatively dosing acetylcholine from 10 nM to 1 mM with ten minute dosing intervals (Fig. 1D). Prior to constriction, the basal tone of healthy and asthmatic phenotypes was not statistically different, a result that may be clinically analogous to the normal specific airway resistance seen in asthmatic children[27]. All stress values were quantified as the difference from the basal tone, denoted as Δ Stress (Fig. 1E). The tissues exposed to IL-13 generated greater stress, as indicated by the traces of the contractions over time in Fig. S2, at each dose of acetylcholine (10 nM-1 mM) when compared to healthy phenotype at the same dose (Fig. 1E). This increased contractile response in our IL-13 induced asthmatic phenotype corresponds with elevated agonist-induced increases in cellular stiffness in human and rabbit

airway smooth muscle measured with atomic force microscopy and magnetic twisting cytometry[28, 29]. These data suggest IL-13 exposure does not increase the basal tone, but induces hypercontraction of human BSM in response to acetylcholine. Thus, bMTFs model a hallmark pathological feature of asthma related to hypercontraction of BSM.

Physiological and impaired relaxation in asthma

Clinically, asthma is distinguished from other obstructive airway diseases by the reversibility of airway obstruction in response to β-agonists [30], such as albuterol and isoproterenol, which induce relaxation by reducing intracellular calcium through production of cyclic adenosine monophosphate (cAMP) [31]. We asked if we could recapitulate these responses in our airway on a chip model. Healthy and IL-13 treated bMTFs were peeled and assumed a basal tone (Fig. 2A–B). Next, 100 μM isoproterenol and 1 mM isoproterenol doses were administered to the tissues in order to induce relaxation. The IL-13 induced asthmatic phenotype had a greater magnitude of relaxation in response to 1 mM isoproterenol compared to the healthy phenotype, indicating IL-13 alone does not cause impaired relaxation of human BSM although it has been shown to reduce the ISO-induced reduction of cell stiffness[32].

Despite the clinical success of β-agonists and glucocorticoids in the majority of asthma patients, 5% to 10% are non-responsive to these therapies and are at a greater risk for hospitalization[7, 33]. Previous work in animals has shown functional antagonism between cholinergic-induced contraction and β-agonist-induced relaxation[34, 35]. We sought to determine if one reason for impaired BSM relaxation in therapy-resistant patients is exposure to specific cytokines and subsequent triggering of intracellular signaling by acetylcholine as IL-13 has been shown to reduce ISO induced relaxation in acetylcholine-preconstricted rabbit airway smooth muscle[29]. To determine the effect of acetylcholine on isoproterenol-induced relaxation in our engineered human tissues, we constricted tissues with acetylcholine prior to inducing relaxation and compared this response to tissues that were relaxed from their basal tone. We peeled the healthy and IL-13 treated bMTFs, allowing them to assume a basal tone (Fig. 2C), and then constricted the tissues using 100 nM acetylcholine. Next, the muscarinic antagonist and bronchodilator atropine was administered to prevent any further contraction due to acetylcholine binding to muscarinic receptors, as well as to induce relaxation to a stress level near the initial basal tone (Fig. 2C). Further relaxation was induced using 100 μM and 1 mM isoproterenol, and the magnitude of relaxation was quantified by calculating the difference of stress after the 1 mM isoproterenol dosing interval and the 50 μM atropine dosing interval (Fig. 2D). The healthy phenotypic tissues constricted with acetylcholine prior to induction of relaxation with isoproterenol did not have a statistically different magnitude of relaxation compared to the healthy phenotype that had not been constricted prior to induction of relaxation (Fig. 2E). However, the IL-13 induced asthmatic phenotypic tissues constricted prior to induction of relaxation had a significant decrease in the magnitude of relaxation in response to isoproterenol compared to the IL-13 induced asthmatic phenotypic tissues that had not been constricted prior to induction of relaxation (Fig. 2E). These data suggest IL-13 and acetylcholine may act synergistically on the same pathway to disrupt relaxation of human BSM.

Effect of IL-13 on engineered muscle structure and contractile protein expression

Thickening of BSM in the airway wall is a structural hallmark of asthma[36, 37] and potentiates airway narrowing. We asked whether IL-13 induced cellular hypertrophy of human BSM in our system. To test this hypothesis, we stained the actin cytoskeleton and nuclei in confluent tissues after culture and treatment with either IL-13 or vehicle (Fig. 3A). We then determined the number of cells per field of view as a measure of average cell under the assumption of confluence (Fig. 3B). The healthy phenotype had a statistically larger number of cells per field of view compared to tissue exposed to IL-13. These results suggest that IL-13 caused increased cellular size of human BSM.

We also asked if IL-13 altered contraction by modifying the organization of the actin cytoskeleton. In the human airway, actin cytoskeletal fibers orient in parallel to the longitudinal axis of the BSM cells[38], which wrap circumferentially around the airway [39, 40]. To investigate tissue architecture, we measured actin orientation angles using an algorithm based on fingerprint identification [41] and quantified their global alignment by calculating the orientational order parameter (OOP), where 1 represents perfect alignment and 0 represents random organization [42] (Fig. 3C). Both healthy and IL-13 induced asthmatic phenotypes had high values of OOP, suggesting highly aligned tissues, reminiscent of BSM in human airway[39, 40]. The IL-13 induced asthmatic phenotype had a greater OOP than the healthy phenotype, indicating IL-13 induced increased alignment of actin fibers.

Next, we asked whether IL-13 altered expression of proteins that regulate contraction in bronchial smooth muscle. Expression of α-smooth muscle actin and smooth muscle myosin heavy chain are thought to be indicative of the contractile phenotype of airway smooth muscle[43]. To determine whether a phenotypic switch contributed to hypercontraction of the tissues exposed to IL-13 in our system, we used Western blots to determine the normalized expression of α-smooth muscle actin in the IL-13 induced asthmatic and healthy phenotypes. The contractile phenotype was supported by observation of diffuse expression of α-smooth muscle actin in immunostained images (Fig. S3A), but there was no statistical difference between protein expression in the healthy and asthmatic conditions (Fig. S3B). Upregulation of the RhoA/ROCK pathway has been implicated as a key player in augmented bronchoconstriction in asthma [44, 45]. Here, we asked if the RhoA/ROCK pathway acts as an effector of hypercontraction of BSM in human asthma. We used Western blots to determine the normalized expression of RhoA and ROCK2 relative to β actin (Fig. 3D). IL-13 induced statistically greater expression of RhoA in the IL-13 induced asthmatic phenotype compared to the healthy phenotype (Fig. 3E), similar to previous reports[32, 44]. However, the increased expression of ROCK2, a downstream effector of RhoA in the IL-13 induced asthmatic phenotype was not found to be statistically significant. These results suggest that the hypercontraction of the IL-13 induced asthmatic phenotype observed in our system may be induced through upregulation of RhoA.

Regulation of hypercontraction and impaired relaxation by the RhoA/ROCK pathway

The contractile strength of smooth muscle is dependent on the intracellular concentration of calcium and calcium sensitization mediated through RhoA [46]. Since we observed that IL-13-induced upregulation of RhoA, we asked if pretreatment with HA1077, an inhibitor of Rho-

mediated calcium sensitization and contraction, would prevent hypercontraction as seen in IL-13-treated mouse BSM[44] and ovalbumin-sensitized guinea pigs[47]. To test this hypothesis, we pretreated the IL-13 induced asthmatic phenotype with 10 μM HA1077 for fifteen minutes in serum-free culture media and washed the drug out with PBS thirty minutes prior to initiation of the acetylcholine dose response. The IL-13 induced asthmatic phenotypic tissues that were pretreated with HA1077 exhibited a statistically lower basal tone than both the healthy phenotype and untreated, IL-13 induced asthmatic phenotype (Fig. 4A and Fig. S4). HA1077-pretreated, IL-13 induced asthmatic phenotypic tissues additionally exhibited statistically lower stresses than both the healthy and untreated IL-13 induced asthmatic phenotypic tissues up to 1 μM acetylcholine (Fig. 4A). For the doses of 10 μM to 1 mM acetylcholine, HA1077-pretreated tissues exposed to IL-13 did not have statistically different stresses compared to the healthy phenotype, but did have statistically lower stress compared to untreated tissues exposed to IL-13 (Fig. 4A). This result indicates HA1077 decreases the basal tone of our engineered BSM tissue and prevents hypercontraction.

Next, we asked whether inhibiting rho kinase would also be effective for inducing relaxation. Similar to the relaxation studies performed using isoproterenol, we peeled the bMTFs, allowed them to assume a basal tone, and then induced relaxation with 10 μM and 100 μM HA1077 (Fig. 4B). Similar to the results of the isoproterenol-induced relaxation without prior constriction (Fig. 2B), HA1077 induced a statistically greater relaxation of the IL-13 induced asthmatic phenotype compared to the healthy phenotype (Fig. 4C). Additionally, we compared the efficacy of 100 μM HA1077 to the efficacy of 1 mM isoproterenol (Fig. 4C). For both healthy and the IL-13 induced asthmatic phenotypes, HA1077 elicited a statistically greater relaxation compared to the isoproterenol-induced relaxation.

Because isoproterenol and HA1077 induce relaxation via different mechanisms, we asked whether using both drugs together would have additive effects. To test this hypothesis, we administered 100 μM isoproterenol, 1 mM isoproterenol, 10 μM HA1077, and 100 μM HA1077 at fifteen minute intervals and measured the decrease in stress relative to the basal tone (Fig. 4D). Additionally, we tested the additive effects of isoproterenol and HA1077 of healthy and the IL-13 induced asthmatic phenotypes that had been constricted with acetylcholine prior to inducing relaxation (Fig. 4E). The magnitude of relaxation was measured as the difference of stress after the 100 μM HA1077 dosing interval and the basal tone (Fig. 4E). In non-constricted tissues, we found the serial dosing of isoproterenol and HA1077 induced significantly greater relaxation in the IL-13 induced asthmatic phenotype compared to the healthy phenotype (Fig. 4D, F). However, in constricted tissues, the IL-13 induced asthmatic phenotype had significantly less relaxation compared to the healthy phenotype (Fig. 4E–F). The constricted, IL-13 induced asthmatic phenotype also had significantly less relaxation compared to non-constricted, IL-13 induced asthmatic phenotype, while the constricted, healthy phenotype relaxed significantly more than the non-constricted, healthy phenotype (Fig. 4D–F). These data indicate IL-13 and acetylcholine act synergistically to alter the ability of asthmatic human BSM to relax. Lastly, we found using both isoproterenol and HA1077 improved relaxation compared to tissues relaxed with isoproterenol alone.

Discussion

The challenge of organ on chips is to recapitulate healthy and diseased physiology of multiple tissue or organ mimics that communicate *in vitro* in order to supplement animals in preclinical drug development [48]. Developing platforms that allow for acquisition of robust, reliable tissue or organ-level structural and functional outputs while maintaining the simplicity requisite for high throughput fabrication is an immense challenge. In this study, we designed, built, and tested an *in vitro* model of healthy and asthmatic human airway musculature. On our human airway musculature chip, we demonstrated that we could recapitulate many of the hallmark clinical features of asthmatic airway smooth muscle: hyperresponsiveness to acetylcholine, physiological and impaired relaxation in distinct experiments, cellular remodeling, and increased expression of contractile proteins. We tested our system using standard airway drugs and observed appropriate functional responses to β-agonists and muscarinic antagonists. Further, we demonstrated the efficacy of HA1077 in prevention of ACh triggered hypercontraction of IL-13 treated tissues and relaxing the muscle from its basal tone and after contraction as well as showed that HA1077 had an additive effect with isoproterenol in inducing relaxation of human airway musculature.

Reversible airway narrowing in asthma elicits the clinical symptoms of breathlessness, wheezing, and coughing [2, 25]. In asthma, the BSM is hyperresponsive to a number of nonspecific stimuli such as tobacco smoke [49], air pollution [50], cleaning agents [51], and drugs such as non-steroidal anti-inflammatories [52]. Clinically, hyperresponsiveness is assessed using spirometry after exposing the airway to the cholinergic agonist methacholine[26]. In this study, the IL-13 induced asthmatic phenotype did not have statistically different basal tone compared to the healthy phenotype but generated greater contractile stress in response to doses of 10 nM to 1 mM of acetylcholine, potentially explaining why asthmatic patients have increased reductions in FEV1 measurements compared to healthy patients [26]. These results indicate that IL-13 does not increase human BSM tone alone but instead acts synergistically with acetylcholine to cause hypercontraction. This result may explain why using the synthetic muscarinic antagonist ipratropium bromide as an adjunct to β agonists has successfully reduced asthmatic exacerbation rates in asthma patients [53].

Episodes of excessive airway narrowing are typically managed using β agonists [53]. Here, we tested the relaxation capability of healthy and the IL-13 induced asthmatic phenotypes using the β agonist isoproterenol. First, the tissues were relaxed from their basal tone, and the IL-13 induced asthmatic phenotype achieved a greater magnitude of relaxation compared to the healthy phenotype. This result suggests that IL-13 alone does not alter the relaxation response of bronchial smooth muscle. However, when we tested relaxation after acetylcholine-induced constriction, the constricted, IL-13 induced asthmatic phenotype had significantly less relaxation compared to the IL-13 induced asthmatic phenotype that had not been constricted. The same effect was not observed in constricted healthy phenotypic tissues. Together, these results indicate that synergism occurs between IL-13 and acetylcholine to alter the relaxation response to isoproterenol. Similar functional antagonism between cholinergic-induced contraction and β agonist-induced relaxation has been observed in canine and guinea pig airway smooth muscle [34, 35], which may be due to inhibition of β agonist-induced cAMP production [54]. Here, the impaired relaxation may

manifest when both acetylcholine disables cAMP regulation of intracellular calcium and IL-13 upregulation of the Rho/ROCK pathway, consequently causing increased intracellular calcium and increased calcium sensitivity.

Structural remodeling is an additional clinical hallmark of the asthmatic human airway[36, 37]. Further, the severity of asthma is related to the extent of airway remodeling [37]. In this study, we found that IL-13 caused increased cellular size within the tissue. Additionally, an increased alignment of actin fibers within tissue treated with IL-13 was observed. Many studies provide evidence indicating that phosphorylation of myosin light chain and remodeling of the actin cytoskeleton possess independent roles in the contraction of smooth muscle [55], where maximum stress generation may be dependent both on length of actin fibers and myosin light chain phosphorylation. Thus, the structural remodeling of BSM cells may play an important role in hypercontraction in asthma.

Protein expression is commonly used to assess the phenotype of smooth muscle in disease. Expression of α-smooth muscle actin and smooth muscle myosin heavy chain are thought to be indicative of a contractile phenotype of airway smooth muscle[43]. Increased expression of RhoA and coupling to ROCK has been associated with diseases involving hypercontraction of smooth muscle like subarachnoid hemorrhage induced vasospasm and asthma [45]. In this study, the increased expression of RhoA in the IL-13 induced asthmatic phenotype was consistent with pathologically hypercontractile smooth muscle tissue.

Lastly, we evaluated newly proposed treatment strategies, specifically HA1077, as a treatment for preventing hypercontraction of human BSM as well as a treatment for acute bronchoconstriction. Pretreatment of the IL-13 induced asthmatic phenotype with HA1077 caused decreased basal tone compared to both healthy and the non-treated, IL-13 induced asthmatic phenotype. Further, this treatment lowered the maximal contractile response of the IL-13 induced asthmatic phenotype, suggesting that upregulation of the Rho/ROCK pathway plays a critical role in hypercontraction of human bronchial smooth muscle. We found that HA1077 induced greater relaxation in both healthy and IL-13 tissues than isoproterenol. Because isoproterenol and HA1077 act on regulation of intracellular calcium and calcium sensitivity, respectively, we tested the additive effects of relaxing both non-constricted and constricted tissues. This resulted in greater relaxation in constricted healthy phenotypic tissues relative to non-constricted healthy phenotypic tissues, while prior constriction reduced the ability of the IL-13 induced asthmatic phenotypes compared to the non-constricted, IL-13 induced asthmatic phenotype. This demonstrates synergism between acetylcholine and IL-13 in altering relaxation capacity. Importantly, it was additionally demonstrated that isoproterenol and HA1077 together induce greater relaxation compared to isoproterenol, the current standard treatment. Clinically, ROCK inhibitors are being considered for treatment of a number of diseases including cerebral vasospasm, glaucoma, cancer, and cardiovascular disease[56–58].

Human organs on chips are of interest because of their promising potential to replace *in vivo* animal studies due to improved specificity, sensitivity, and predictiveness[59]. Our work represents the next stage of development where we build more fidelity into our system by mimicking disease. This is important for drug safety and efficacy testing and disease

modeling as well as mechanism-based search for therapeutics. Further, the airway musculature on a chip is amenable to integration into microfluidic system which will enable coupling with other healthy and diseased organ mimics.

Experimental

Chip Fabrication

Glass coverslips (22 mm × 22 mm, VWR, Westbury NY, catalog# 48366-067) were cleaned in 70% ethanol via sonication for thirty minutes and subsequently air dried. A piece of low adhesion Scotch tape (3M, St. Paul, MN) was applied to cover the entire surface of the glass coverslip. Two rectangles with rounded corners with dimensions of 13 mm × 5.5 mm were laser engraved into the tape using a CO_2 laser (VersaLaser 2.0, 10.6 μm wavelength, 10 W, Universal Laser systems, Scottsdale, AZ) using 10% power and 2% speed settings [23]. The rectangles were then peeled from the coverslip while leaving the remaining surface covered by the tape. A thin layer of poly(N-isopropylacrylamide) (pNIPAAM) (Polysciences, Warrington, PA) dissolved in1-butanol (10% w/v) was spin coated at a maximum speed of 6000 RPM for one minute onto the exposed areas of the coverslip in order to serve as a sacrificial layer. After removing the remaining tape, Polydimethylsiloxane (PDMS) (Sylgard 184, Dow Corning, Midland, MI) was mixed at a 10:1 base to curing agent ratio and spin coated at a maximum speed of 4000 RPM for one minute so that a thin layer of PDMS coated both the uncoated and pNIPAAM-coated regions of the coverslip. After curing of the PDMS layer over night at 65°C, two rows of six cantilevers with dimensions of 2 mm × 5 mm were laser engraved (Laser cutter settings: 0.2% power and 0.1% speed) [23] into the regions consisting of both pNIPAAM and PDMS layers.

Cell Culture

Normal human BSM cells (Lonza, Walkersville, MD) were purchased at passage two and cultured in growth medium consisting of M199 culture medium (GIBCO, Invitrogen, Carlsbad, CA) supplemented with 10% heat inactivated fetal bovine serum, 10 mM HEPES, 0.1 mM MEM nonessential amino acids, 20 mM glucose, 1.5 μM vitamin B-12, 50 U mL^{-1} penicillin, and 50 U mL^{-1} streptomycin (GIBCO) [22]. Cells were allowed to proliferate in tissue culture flasks until they reached 70–80% confluence. Experiments were performed using cells from passage 5–7. The cells were trypsinized with 0.25% of trypsin-EDTA (GIBCO), seeded onto chips at a density of 25,000 cells cm^{-2}, and cultured in the growth media for 48 hours to form a confluent tissue. The growth media was then replaced with a serum free media of M199, supplemented with 10 mM HEPES, 0.1 mM MEM nonessential amino acids, 20 mM glucose, 1.5 μM vitamin B-12, 50 U mL^{-1} penicillin, and 50 U mL^{-1} streptomycin for 24 hours to induce a contractile phenotype [21]. After 24 hours, induction of the asthmatic phenotype was achieved by supplementing the serum free media with 100 ng mL^{-1} human IL-13 (Sigma-Aldrich) during the final 10–14 hours of culture prior to experiments. Interleukin-13 was reconstituted in 20 mM acetic acid at a concentration of 0.1 mg mL^{-1} then further diluted to 1 μg 1 mL^{-1} in 0.1% BSA for long term storage at −20 °C per the vendor specifications. The vehicle, consisting of 20 mM acetic acid diluted in 0.1% BSA, was added to the control tissue. The tissues were triple rinsed with PBS prior to experiments.

Contractility Experiments

bMTF experiments were performed on a Leica MZ9.5 stereomicroscope (Wetzlar, Germany) with 0.63X magnification, coupled to a National Instruments LabVIEW data acquisition board which was programmed to capture the horizontal projection of the films by taking an image every 30 seconds through the course of the experiment using a Basler A601f-2 camera (Exton, PA). bMTF chips were transferred to a 35 mm Petri dish containing Tyrode's solution (1.8 mM $CaCl_2$, 5 mM glucose, 5 mM HEPES, 1 mM $MgCl_2$, 5.4 mM of KCl, 135 mM of NaCl, and 0.33 mM of NaH_2PO_4 in deionized water, pH 7.4 at 37 °C; reagents from Sigma-Aldrich). Tyrode's solution was allowed to cool below 32 °C to allow dissolution of the pNIPAAM layer. The bMTFs were then gently peeled and the dish was placed in a heated plate to re-equilibrate to 37 °C, allowing the films to reach a basal tone. For contractile studies, contraction was induced with cumulative dosing of acetylcholine chloride (Sigma-Aldrich) (ACh) dissolved in distilled water: 10 nM ACh, 100 nM ACh, 1 μM ACh, 10 μM ACh, 100 μM ACh, and 1mM ACh at ten minute intervals.

Relaxation Experiments

For relaxation, there were two types of studies: relaxation without preconstriction and relaxation after preconstriction. For relaxation without preconstriction, the bMTFs were peeled and allowed to achieve a basal tone as done in contractility experiments. Relaxation was then induced using cumulative dosing of isoproterenol (100 μM and 1 mM) (Sigma-Aldrich) dissolved in distilled water, dosing 15 minutes after previous dose. For relaxation after preconstriction, the bMTFs were released to their basal tone and then induced to contract with 100 nM ACh. Next, 50 μM atropine (Sigma-Aldrich) dissolved in water was added to induce relaxation and prevent further contraction. Further relaxation was induced using cumulative dosing of 100 μM isoproterenol and 1 mM isoproterenol with 15 minutes between doses.

Rho Kinase Inhibition Experiments

To test the effect of rho kinase in acetylcholine-induced hypercontraction, asthmatic tissues were pretreated with 10 μM HA1077 (Sigma-Aldrich) for 15 minutes in serum free culture medium. Thirty minutes prior to the contractile experiment, HA1077 was triple washed out using PBS, then moved to Tyrode's solution as described above. To test the relaxation response to HA1077, the bMTFs were peeled and allowed to achieve a basal tone as described, then induced to relax with cumulative dosing of HA1077 (10 μM and 100 μM). To determine whether HA1077 would have an additive effect with isoproterenol, tissues relaxed with cumulative dosing of 100 μM and 1 mM isoproterenol were further relaxed with 10 μM and 100 μM HA1077, with 15 minute intervals between doses.

Microcontact Printing

In order to engineer anisotropic BSM oriented along the longitudinal axis of the thin films, the chips were microcontact printed, as previously published [19, 21, 60]. Briefly, a silicon wafer was coated with a thin layer of SU8-2002 (MicroChem Corporation, Newton, MA), a negative photoresist, via spin coating. After baking the photoresist-coated silicon wafer, a photomask was brought into contact with the wafer using a mask aligner, and UV light was

shown through the mask. Regions exposed to UV light became insoluble and the rest was dissolved away with developer solution. After development, the etched wafer served as a template for fabrication of PDMS stamps. PDMS stamps with 15 μm lines and 2 μm spacing were incubated with 200 μl of human fibronectin (BD Biosciences, Sparks, MD) at 50 μg mL^{-1} in distilled water for one hour. Excess fibronectin was air blown from the PDMS stamp and applied to the chip which had been recently exposed to UV ozone (Model# 342, Jelight Company Inc., Phoenix, AZ) for eight minutes in order to transiently switch the substrate to a hydrophilic state. Stamps were manually positioned so that lines were oriented along the longitudinal axis of the thin films. Seeding of cells occurred immediately after microcontact printing.

Western Blotting

Tissues were lysed in urea lysis buffer consisting of 100 mM Tris, 4 M urea, 5 mM EDTA, 0.5% SDS, 0.5% NP-40 (Sigma-Aldrich), and Halt Protease and Phosphatase Inhibitor Cocktail (Thermo Scientific, Rockford, IL). Licor TG-SDS running buffer (Lincoln, NE) was used for electrophoresis. Protein concentration was quantified using a bicinchoninic acid assay and a SpectraMaxM2e microplate reader (Molecular Devices, Vienna, VA). 10 μg of total protein was loaded into Criterion 4–15% polyacrylamide gels (Bio-Rad, Hercules, CA) and the gel was run for 90 minutes at 120 V. The gel was transferred to PVDF membranes (Licor) at 70 V for 40 minutes for Western analysis. Membranes were incubated in primary antibody diluted in PBS and Licor blocking buffer for 48 hours at 4°C. Primary antibodies used were α-smooth muscle actin (1:200 dilution, Abcam, Cambridge, MA), ROCK2 (1:50 dilution, Santa Cruz Biotechnology, Santa Cruz, CA), RhoA (1:200 dilution, Santa Cruz Biotechnology, Santa Cruz, CA), and β actin (1:1000 dilution, Santa Cruz Biotechnology, Santa Cruz, CA). Secondary antibodies were conjugated with infrared labels (1:1000 dilution, Licor, Lincoln, NE) and imaged with a Licor Odyssey reader (Licor, Lincoln, NE). Densitometry analysis was carried out using Odyssey 3.0 software and ImageJ (NIH, Bethesda, MD) and the quantified values were compared using the student's t-test.

Actin alignment quantification

Engineered tissues were fixed with 4% paraformaldehyde (16% stock diluted in PBS, Electron Microscopy Sciences, Hatfield, PA) for 10 minutes and subsequently permeabilized with 0.05% Triton X-100 (Sigma-Aldrich) for 12 minutes. Tissues were triple rinsed with PBS. These fixed and permeabilized tissues were stained with the Alexa Fluor 488-conjugated Phalloidin (Product# A12379 Invitrogen, Carlsbad, CA) and 4′, 6-diamidino-2-phenylindole (DAPI) (Catalog #D1306, Invitrogen, Carlsbad, CA) [21]. Ten randomly chosen fields of view for each coverslip were imaged on an inverted light microscope (Leica DMI 6000B, Wetzlar, Germany) in epifluorescence using a 40x objective lens and a Coolsnap HQ CCD camera (Roper Scientific, Tucson, AZ) controlled by IPLab Spectrum (BD Biosciences/Scanalytics, Rockville, MD). Custom MATLAB software (MathWorks, Natick, MA) based on fingerprint detection, as previously reported [20, 21], was used to threshold actin immmunosignals and detect the orientation angles of continuous pixel segments. The orientation angles were consolidated for each tissue for calculation of the orientational order parameter (OOP) [20], where 1 represents perfect alignment and 0

represents random organization [42]. Quantified values were compared using the student's t-test.

Calculation of bMTF Tissue Stress

bMTF tissue stresses were calculated using previously published methods [19, 20]. Images of bMTFs were thresholded using custom ImageJ (NIH, Bethesda, Maryland) software, as previously described [20]. MATLAB software (MathWorks, Natick, MA) was used to calculate the stress generated by each film based on the horizontal projection of the radius of curvature, thickness of the PDMS film, and tissue layer thickness, using methods previously described [20]. The thickness of the PDMS thin films was determined using a contact profilometer (Dektak 6M, Veeco Instruments Inc., Plainview, NY). F-actin was stained with Alexfluor 488 phalloidin (Product# A12379 Invitrogen, Carlsbad, CA) and local thickness was measured using the z-plane projections of f-actin filaments using a Zeiss LSM 5 LIVE confocal microscope with a Plan-Neofluar 40X/1.3 oil objective. Contractility experiments comparing stress values of healthy and IL-13 exposed tissue at each concentration of acetylcholine failed the Shapiro-Wilkinson test for normality and were thus statistically evaluated using the Mann-Whitney Rank Sum Test. For contractility experiments comparing the stress values of healthy tissues, IL-13 exposed tissues, and IL-13 exposed tissues pretreated with HA1077, stresses at each concentration failed the Shapiro-Wilkinson test for normality and therefore were evaluated using the Kruskal-Wallis One Way ANOVA on Ranks and compared pairwise using Dunn's Method. Results with p-values less than 0.05 were considered statistically significant.

Statistical Analysis

Contractility experiments comparing stress values of healthy and the IL-13 induced asthmatic phenotypes at each concentration of acetylcholine failed the Shapiro-Wilkinson test for normality and were thus statistically evaluated using the Mann-Whitney Rank Sum Test. For contractility experiments comparing the stress values of the healthy phenotype, the IL-13 induced asthmatic phenotype, and the IL-13 induced asthmatic phenotype pretreated with HA1077, stresses at each concentration failed the Shapiro-Wilkinson test for normality and therefore were evaluated using the Kruskal-Wallis One Way ANOVA on Ranks and compared pairwise using Dunn's Method. Results with p-values less than 0.05 were considered statistically significant.

Conclusions

We utilized a laser-based fabrication technique to build an airway musculature chip amenable quantification of pathological structural and functional changes at the subcellular, cellular, and tissue levels. We recapitulated key clinical hallmarks of asthma seen in patients and replicated results seen in animal and other *in vitro* systems while also achieving high throughput. Muscular thin films, in the form of an organ on a chip, are effective for evaluating new pharmaceutical compounds, identifying disease mechanisms, and performing mechanism-based searches for therapeutics.

Supplementary Material

Refer to Web version on PubMed Central for supplementary material.

Acknowledgments

We thank the Harvard Center for Nanoscale Systems for use of cleanroom facilities. We would also like to thank Rene Chen for her contributions on Fig. 1A. This work was funded by National Institutes of Health (UH2 NS080728-01) and Harvard School of Engineering and Applied Sciences.

References

1. Akinbami LJ, Schoendorf KC. Pediatrics. 2002; 110:315–322. [PubMed: 12165584]
2. Kuperman DA, Huang X, Koth LL, Chang GH, Dolganov GM, Zhu Z, Elias JA, Sheppard D, Erle DJ. Nature Medicine. 2002; 8:885–889.
3. Barnes PJ. Journal of Clinical Investigation. 2008; 118:3546–3556. [PubMed: 18982161]
4. Guilbert TW, Morgan WJ, Zeiger RS, Mauger DT, Boehmer SJ, Szefler SJ, Bacharier LB, Lemanske RF, Strunk RC, Allen DB, Bloomberg GR, Heldt G, Krawiec M, Larsen G, Liu AH, Chinchilli VM, Sorkness CA, Taussig LM, Martinez FD. The New England Journal of Medicine. 2006; 354:1985–1997. [PubMed: 16687711]
5. Barnes PJ, Adcock IM. Lancet. 2009; 373:1905–1917. [PubMed: 19482216]
6. Saha SK, Berry MA, Parker D, Siddiqui S, Morgan A, May R, Monk P, Bradding P, Wardlaw AJ, Pavord ID, Brightling CE. Journal of Allergy and Clinical Immunology. 2008; 121:685–691. [PubMed: 18328894]
7. Corren J, Lemanske RF, Hanania NA, Korenblat PE, Parsey MV, Arron JR, Harris JM, Scheerens H, Wu LC, Su Z, Mosesova S, Eisner MD, Bohen SP, Matthews JG. The New England Journal of Medicine. 2011; 365:1088–1098. [PubMed: 21812663]
8. Mullane K. Biochemical Pharmacology. 2011; 82:586–599. [PubMed: 21745459]
9. Zosky GR, Sly PD. Clinical and Experimental allergy:Journal of the British Society for Allergy and Clinical Immunology. 2007; 37:973–988. [PubMed: 17581191]
10. van der Worp HB, Howells DW, Sena ES, Porritt MJ, Rewell S, O'Collins V, Macleod MR. PLoS Medicine. 2010; 7:e1000245. [PubMed: 20361020]
11. Wright D, Sharma P, Ryu MH, Risse PA, Ngo M, Maarsingh H, Koziol-White C, Jha A, Halayko AJ, West AR. Pulmonary Pharmacology & Therapeutics. 2013; 26:24–36. [PubMed: 22967819]
12. Wang N, Tolic-Norrelykke IM, Chen J, Mijailovich SM, Butler JP, Fredberg JJ, Stamenovic D. American Journal of Physiology - Cell Physiology. 2002; 282:C606–616. [PubMed: 11832346]
13. Fabry B, Maksym GN, Shore SA, Moore PE, Panettieri RA, Butler JP, Fredberg JJ. Journal of Applied Physiology. 2001; 91:986–994. [PubMed: 11457818]
14. An SS, Kim J, Ahn K, Trepat X, Drake KJ, Kumar S, Ling G, Purington C, Rangasamy T, Kensler TW, Mitzner W, Fredberg JJ, Biswal S. Biochemical and Biophysical Research Communications. 2009; 382:697–703. [PubMed: 19327344]
15. West AR, Zaman N, Cole DJ, Walker MJ, Legant WR, Boudou T, Chen CS, Favreau JT, Gaudette GR, Cowley EA, Maksym GN. American Journal of Physiology Lung Cellular and Molecular Physiology. 2013; 304:L4–16. [PubMed: 23125251]
16. Humbert M, Durham SR, Kimmitt P, Powell N, Assoufi B, Pfister R, Menz G, Kay AB, Corrigan CJ. The Journal of Allergy and Clinical Immunology. 1997; 99:657–665. [PubMed: 9155833]
17. Prieto J, Lensmar C, Roquet A, Van der Ploeg I, Gigliotti D, Eklund A, Grunewald J. Respiratory Medicine. 2000; 94:806–814. [PubMed: 10955758]
18. Feinberg AW, Feigel A, Shevkoplyas SS, Sheehy S, Whitesides GM, Parker KK. Science. 2007; 317:1366–1370. [PubMed: 17823347]
19. Alford PW, Feinberg AW, Sheehy SP, Parker KK. Biomaterials. 2010; 31:3613–3621. [PubMed: 20149449]

20. Grosberg A, Alford PW, McCain ML, Parker KK. Lab on a Chip. 2011; 11:4165–4173. [PubMed: 22072288]
21. Alford PW, Nesmith AP, Seywerd JN, Grosberg A, Parker KK. Integrative Biology: Quantitative Biosciences from Nano to Macro. 2011; 3:1063–1070. [PubMed: 21993765]
22. Alford PW, Dabiri BE, Goss JA, Hemphill MA, Brigham MD, Parker KK. Proceedings of the National Academy of Sciences of the United States of America. 2011; 108:12705–12710. [PubMed: 21765001]
23. Agarwal A, Goss JA, Cho A, McCain ML, Parker KK. Lab on a Chip. 201310.1039/c3lc50350j
24. Grainge CL, Lau LCK, Ward JA, Dulay V, Lahiff G, Wilson S, Holgate S, Davies DE, Howarth PH. The New England Journal of Medicine. 2011; 364:2006–2015. [PubMed: 21612469]
25. Sumino K, Sugar EA, Irvin CG, Kaminsky DA, Shade D, Wei CY, Holbrook JT, Wise RA, Castro M, Re ALAAC. Journal of Allergy and Clinical Immunology. 2012; 130:69. [PubMed: 22465214]
26. Boonsawat W, Salome CM, Woolcock AJ. The American Review of Respiratory Disease. 1992; 146:565–569. [PubMed: 1519829]
27. Badier M, Guillot C, Dubus JC. Pediatric Pulmonology. 1999; 27:117–123. [PubMed: 10088935]
28. Risse PA, Jo T, Suarez F, Hirota N, Tolloczko B, Ferraro P, Grutter P, Martin JG. American journal of physiology Lung Cellular and Molecular Physiology. 2011; 300:L958–966. [PubMed: 21460123]
29. Grunstein MM, Hakonarson H, Leiter J, Chen M, Whelan R, Grunstein JS, Chuang S. American journal of physiology Lung Cellular and Molecular Physiology. 2002; 282:L520–528. [PubMed: 11839548]
30. Dekker FW, Schrier AC, Sterk PJ, Dijkman JH. Thorax. 1992; 47:162–166. [PubMed: 1519192]
31. Johnson M. The Journal of Allergy and Clinical Immunology. 2006; 117:18–24. quiz 25. [PubMed: 16387578]
32. Laporte JC, Moore PE, Baraldo S, Jouvin MH, Church TL, Schwartzman IN, Panettieri RA Jr, Kinet JP, Shore SA. American Journal of Respiratory and Critical Care Medicine. 2001; 164:141–148. [PubMed: 11435252]
33. Bateman ED, Boushey HA, Bousquet J, Busse WW, Clark TJH, Pauwels RA, Pedersen SE, Grp GI. American Journal of Respiratory and Critical Care Medicine. 2004; 170:836–844. [PubMed: 15256389]
34. Fernandes LB, Fryer AD, Hirshman CA. Journal of Pharmacology and Experimental Therapeutics. 1992; 262:119–126. [PubMed: 1625190]
35. Watson N, Eglen RM. British Journal of Pharmacology. 1994; 112:179–187. [PubMed: 8032639]
36. Ebina M, Takahashi T, Chiba T, Motomiya M. American Review of Respiratory Disease. 1993; 148:720–726. [PubMed: 8368645]
37. Chetta A, Foresi A, DelDonno M, Bertorelli G, Pesci A, Olivieri D. Chest. 1997; 111:852–857. [PubMed: 9106559]
38. Togashi H, Emala CW, Hall IP, Hirshman CA. The American Journal of Physiology - Lung Cellular and Molecular Physiology. 1998; 274:L803–L809.
39. James A, Carroll N. The European Respiratory Journal: Official Journal of the European Society for Clinical Respiratory Physiology. 2000; 15:782–789.
40. Lei M, Ghezzo H, Chen MF, Eidelman DH. Journal of Applied Physiology. 1997; 82:70–77. [PubMed: 9029200]
41. Bray MA, Sheehy SP, Parker KK. Cell Motility and the Cytoskeleton. 2008; 65:641–651. [PubMed: 18561184]
42. Volfson D, Cookson S, Hasty J, Tsimring LS. Proceedings of the National Academy of Sciences of the United States of America. 2008; 105:15346–15351. [PubMed: 18832176]
43. Halayko AJ, Salari H, Ma XF, Stephens NL. American Journal of Physiology- Lung Cellular and Molecular Physiology. 1996; 270:L1040–L1051.
44. Chiba Y, Nakazawa S, Todoroki M, Shinozaki K, Sakai H, Misawa M. American Journal of Respiratory Cell and Molecular Biology. 2009; 40:159–167. [PubMed: 18688040]
45. Kudo M, Melton AC, Chen C, Engler MB, Huang KE, Ren X, Wang Y, Bernstein X, Li JT, Atabai K, Huang X, Sheppard D. Nature Medicine. 2012; 18:547–554.

46. Uehata M, Ishizaki T, Satoh H, Ono T, Kawahara T, Morishita T, Tamakawa H, Yamagami K, Inui J, Maekawa M, Narumiya S. Nature. 1997; 389:990–994. [PubMed: 9353125]
47. Schaafsma D, Bos IS, Zuidhof AB, Zaagsma J, Meurs H. American Journal of Physiology- Lung Cellular and Molecular Physiology. 2008; 295:L214–219. [PubMed: 18487358]
48. Capulli AK, Tian K, Mehandru N, Bukhta A, Choudhury SF, Suchyta M, Parker KK. Lab on a Chip. 201410.1039/c4lc00276h
49. Mannino DM, Homa DM, Redd SC. Chest. 2002; 122:409–415. [PubMed: 12171810]
50. Wardlaw AJ. Clinical and Experimental Allergy: Journal of the British Society for Allergy and Clinical Immunology. 1993; 23:81–96. [PubMed: 8448686]
51. Quirce S, Barranco P. Journal of Investigational Allergology and Clinical Immunology. 2010; 20:542–550. quiz 542p following 550. [PubMed: 21313993]
52. Szczeklik A, Nizankowska E. Thorax. 2000; 55(Suppl 2):S42–44. [PubMed: 10992556]
53. Schuh S, Johnson DW, Callahan S, Canny G, Levison H. Journal of Pediatrics. 1995; 126:639–645. [PubMed: 7699549]
54. Sankary RM, Jones CA, Madison JM, Brown JK. The American Review of Respiratory Disease. 1988; 138:145–150. [PubMed: 2849336]
55. Tseng S, Kim R, Kim T, Morgan KG, Hai CM. American Journal of Physiology-Cell Physiology. 1997; 272:C1960–C1967.
56. Pan P, Shen M, Yu H, Li Y, Li D, Hou T. Drug Discovery Today. 2013; 18:1323–1333. [PubMed: 24076262]
57. Wang SK, Chang RT. Clinical Ophthalmology. 2014; 8:883–890. [PubMed: 24872673]
58. Zhao J, Zhou D, Guo J, Ren Z, Zhou L, Wang S, Zhang Y, Xu B, Zhao K, Wang R, Mao Y, Xu B, Zhang XG. Neurologia Medico-Chirurgica. 2011; 51:679–683. [PubMed: 22027241]
59. Huh D, Leslie DC, Matthews BD, Fraser JP, Jurek S, Hamilton GA, Thorneloe KS, McAlexander MA, Ingber DE. Science Translational Medicine. 2012; 4:159ra147.
60. Chen CS, Mrksich M, Huang S, Whitesides GM, Ingber DE. Science. 1997; 276:1425–1428. [PubMed: 9162012]

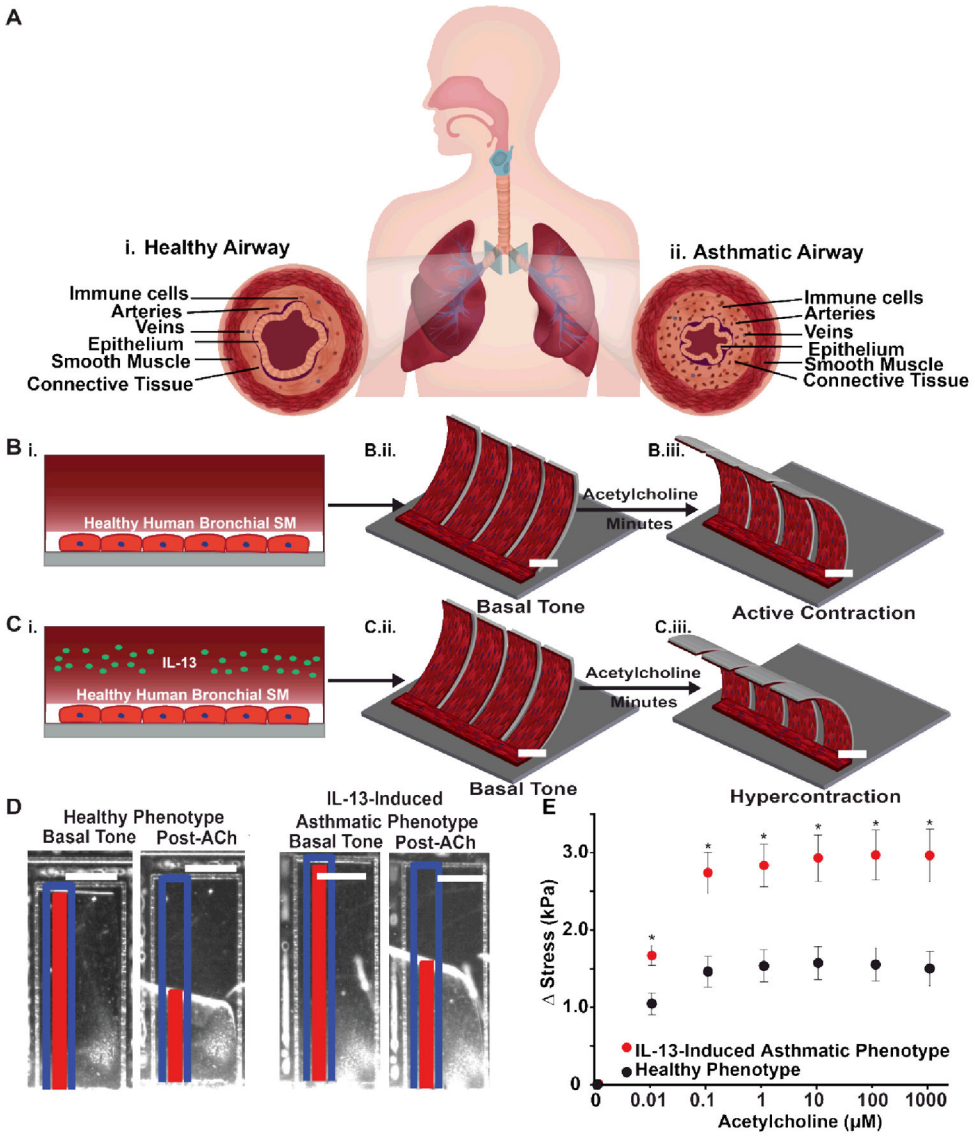

Fig. 1.

Design, build, test: airway musculature on a chip. **(A)** Schematic of the healthy and asthmatic airway. Anisotropic, muscular lamellae wrap around the human airway to control airway tone. (i) The healthy airway is characterized by few immune cells and a patent airway. (ii) The asthmatic airway is characterized by influx of immune cells, structural remodeling, and a constricted airway. **(B)** Schematic depicting acetylcholine-induced contraction of healthy bMTF chip. (i) The healthy airway was recapitulated by engineering anisotropic, muscular lamella on thin films. (ii) The bMTFs are peeled and assumed a basal tone. (iii) Active contraction is induced by administering acetylcholine (ACh). Scale bar represents 2 mm. **(C)** Schematic depicting ACh-induced contraction of asthmatic bMTF chip. (i) The asthmatic airway was recapitulated by administering interleukin 13 (IL-13) to the engineered BSM (BSM) during culture. (ii) The asthmatic bMTFs are peeled and assume a basal tone. (iii) Active contraction is induced by administering ACh. Scale bar represents 2 mm. **(D)** Representative images of bMTFs at basal tone and post-ACh administration. Scale

bar represents 1 mm. The blue outline and red tracker represent the original length and horizontal projection of the film, respectively. **(E)** Stress is plotted against ACh concentration (10 nM to 1 mM) and measured from the initial basal tone. n=15 films, 3 chips for the healthy phenotype; n=23 films, 4 chips for the IL-13 induced asthmatic phenotype. Data points represent mean +/− standard error. * indicates $p<0.05$ at a given dose of ACh.

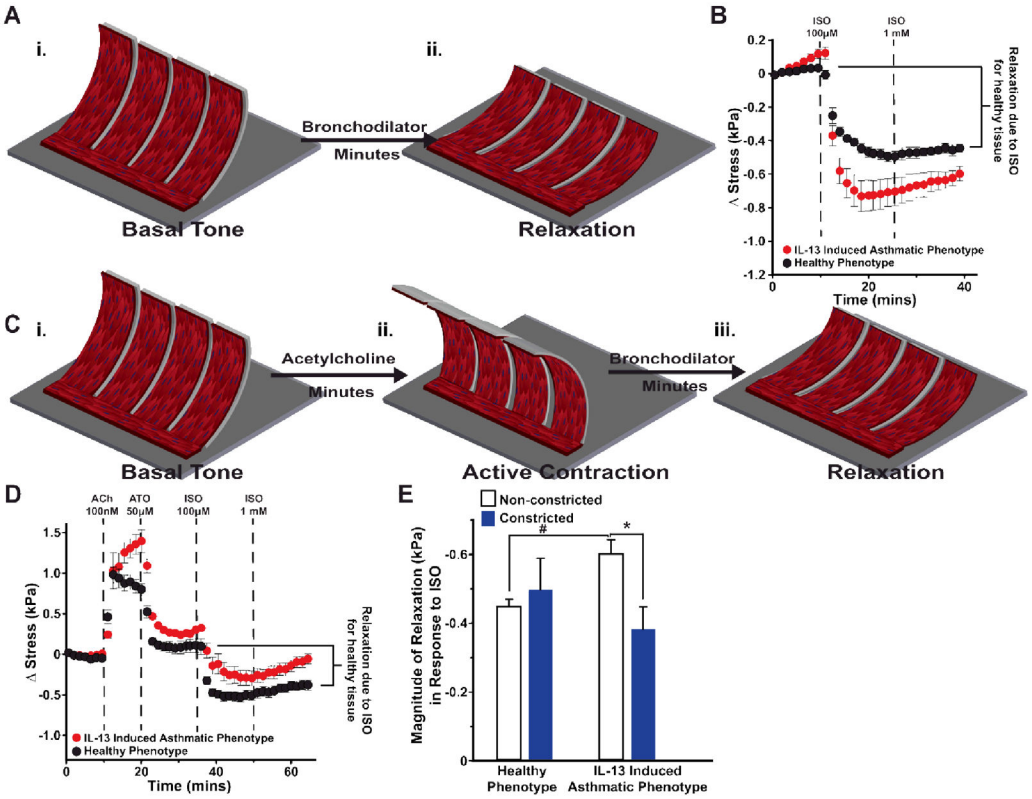

Fig. 2.

Impaired relaxation due to synergistic effect of IL-13 and ACh. **(A)** Schematic depicting (i) the basal tone and (2) bronchodilator-induced relaxation of bMTF chip. **(B)** Relaxation was quantified in response to the β-agonist isoproterenol (ISO). Stress is measured from the basal tone. n=12 films, 2 chips for the healthy phenotype; n=10 films, 2 chips for the IL-13 induced asthmatic phenotype. Data points represent mean ± standard error. **(C)** Schematic depicting (i) basal tone (ii) preconstriction and (iii) bronchodilator-induced relaxation of airway on a chip after initially constricting the tissue. **(D)** Tissues were constricted using ACh then subsequently treated with atropine (ATO) 50 μM, isoproterenol (ISO) 100 μM, and ISO 1 mM in series to induce relaxation. Stress is measured from the basal tone. n=11 films for the healthy phenotype, 2 chips; n=12 films, 2 chips for the IL-13 induced asthmatic phenotype. Data points represent mean ± standard error. **(E)** The magnitude of relaxation in response to ISO was quantified for non-constricted tissues (dark gray) and constricted tissues (black). For non-constricted tissues, the change in stress was measured between the basal tone and the tone after administration of 1 mM ISO (seen in the stress traces in Fig. 2B). For constricted tissues, the change in stress was measured between the tone after administration of 50 μM ATO and the tone after administration of 1 mM ISO (seen in the stress traces in fig. 2D). * and # indicate $p<0.05$.

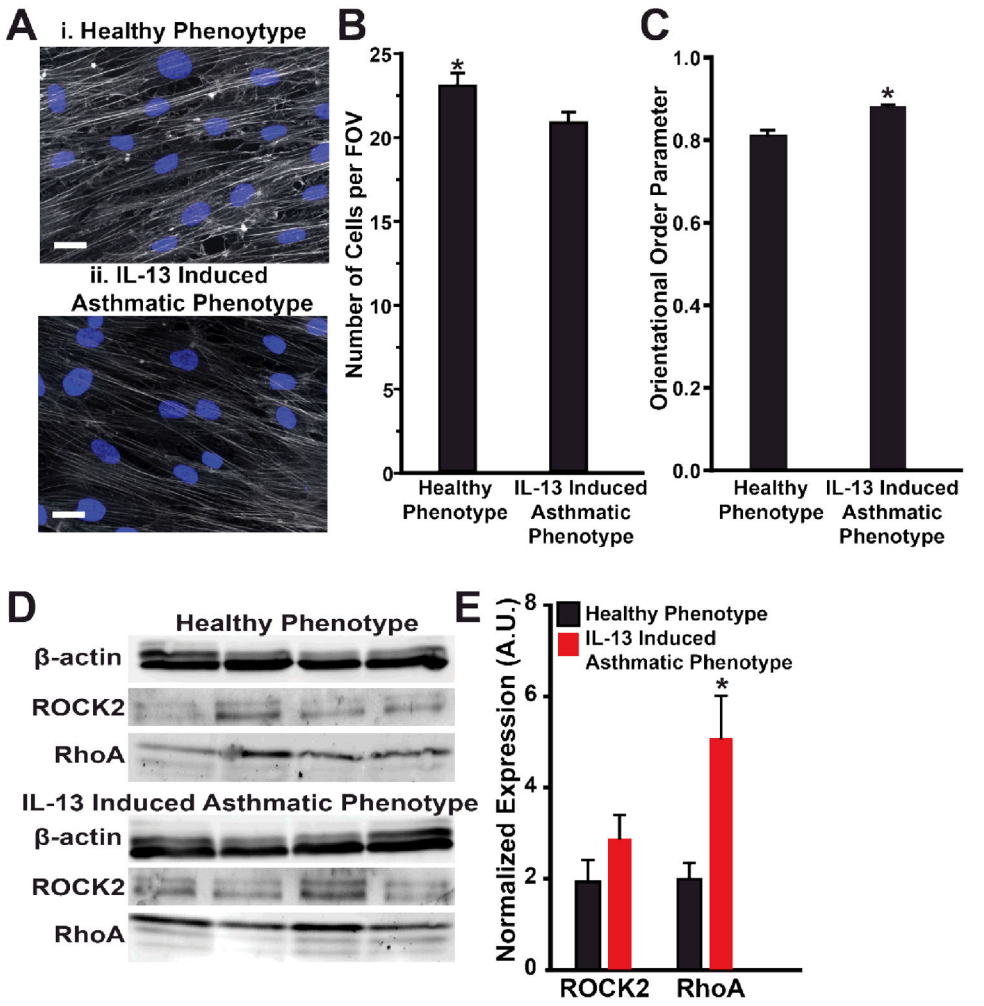

Fig. 3.

Structural and protein expression changes due to IL-13. **(A)** Representative (i) healthy and (ii) IL-13 exposed engineered BSM tissues immunostained for f-actin (gray) and nuclei (blue). Scale bar is 25 μm. **(B)** The average number of cells per field of view (222 μm by 166 μm) was quantified with the assumption each cell had a single nucleus. Mean ± standard error, n=5 chips, for healthy and the IL-13 induced asthmatic phenotypes, 10 fields of view per sample, * indicates $p<0.05$. **(C)** The actin orientational order parameter (OOP) is plotted for each condition. Mean ± standard error, n=5 chips, 10 fields of view per sample for healthy and the IL-13 induced asthmatic phenotypes, * indicates $p<0.05$. **(D)** Western blot gel using β-actin as a control for total protein expression. **(E)** Normalized protein expression, measured by Western blot, for ROCK2 and RhoA. Mean ± standard error, n=4 tissues for each condition, * indicates $p<0.05$.

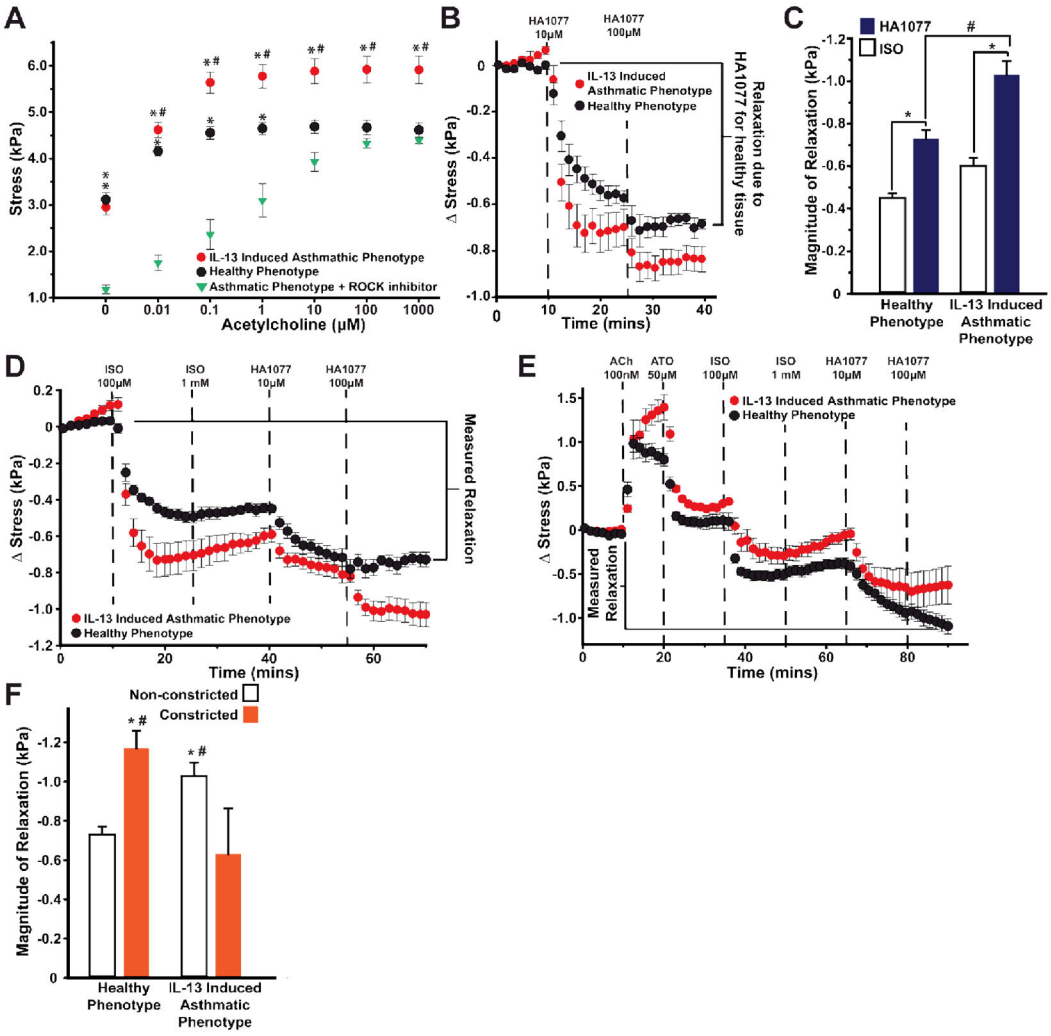

Fig. 4.

Regulation of hypercontraction via the RhoA/ROCK2 pathway. **(A)** The contractile response of the IL-13 induced asthmatic phenotype pretreated with 10 μM HA1077. n=15 films, 3 chips for the healthy phenotype; 4 chips, n=23 films for the IL-13 induced asthmatic phenotype; n=12 films, 2 chips for IL-13 tissue pretreated with HA1077. Data points represent mean ± standard error. The ACh dose response was plotted versus concentration denoting statistical significance at each dose, * indicates $p<0.05$ relative to IL-13 tissue pretreated with HA1077 and # indicates $p<0.05$ relative to both healthy phenotypic tissues and the IL-13 induced asthmatic phenotypic tissues pretreated with HA1077. **(B)** For the healthy and the IL-13 induced asthmatic phenotypes, relaxation was quantified in response to HA1077. Stress is measured from the basal tone. n=12 films for the healthy phenotype, 2 chips; n=12 films, 2 chips for the IL-13 induced asthmatic phenotype. Data points represent mean ± standard error. **(C)** The magnitude of relaxation in response to HA1077 was quantified measuring the change in stress between the basal tone and the tone after the administration of 100 μM HA1077. This response was compared to the relaxation induced in response to 1mM ISO seen in Fig. 2B. * and # indicate $p<0.05$. **(D)** Healthy and the IL-13

induced asthmatic phenotypes were relaxed from the basal tone using ISO and HA1077 in series. Stress is measured from the basal tone. n=10 films, 2 chips for the healthy phenotype; n=11 films, 2 chips for the IL-13 induced asthmatic phenotype. Data points represent mean ± standard error. **(E)** Tissues were constricted using ACh, then relaxed using ATO, ISO, and HA1077 in series. Stress is measured from the basal tone. n=11 films for the healthy phenotype, 2 chips; n=12 films, 2 chips for the IL-13 induced asthmatic phenotype. Data points represent mean ± standard error. **(F)** The relaxation was quantified by measuring the change in stress between the basal tone and the tone after administration of 100 μM HA1077. * indicates $p<0.05$ between non-constricted and constricted tissues within a condition. # indicates $p<0.05$ of the non-constricted/constricted tissues between the healthy and IL-13 conditions.